



Parametric instability-induced synchronization in chemical oscillations and spatiotemporal patternsShibashis Paul , Krishnendu Pal, and Deb Shankar Ray ^{*}
Indian Association for the Cultivation of Science, Jadavpur, Kolkata-700032, India

(Received 24 February 2020; accepted 25 October 2020; published 16 November 2020)

We consider a model reaction-diffusion system with two coupled layers in which one of the components in a layer is parametrically driven by a periodic force. On perturbation of a homogeneous stable steady state, the system exhibits parametric instability inducing synchronization in temporal oscillation at half the forcing frequency in absence of diffusion and spatiotemporal patterns in presence of diffusion, when strength of parametric forcing and the strength of coupling are kept above their critical thresholds. We have formulated a general scheme to derive analytically the critical thresholds and dispersion relation to locate the unstable spatial modes lying between the tilted Arnold tongue in the amplitude-frequency plot. Full numerical simulations on Gierer-Meinhardt activator-inhibitor model corroborate our theoretical analysis on parametric instability-induced antiphase synchronization in chemical oscillation and spatiotemporal pattern formation, between the two layers.

DOI: [10.1103/PhysRevE.102.052209](https://doi.org/10.1103/PhysRevE.102.052209)**I. INTRODUCTION**

Periodic forcing of an excitable or oscillatory system in zero dimension or with spatial extension lies at the heart of nonlinear dynamics [1,2]. An oscillatory system driven by a periodic perturbation with appropriate frequency and amplitude may get entrained where the entrainment occurs for matching of rational ratio of numbers with the frequency ratio of the forcing frequency and the characteristic frequency of the system [3,4]. Periodic forcing of circadian clock in the sleep-wake cycle by sunlight [5–7], of Belousov-Zhabotinsky (BZ) reaction by light [8,9], of electrochemical reaction by potential wave [10] has opened up a variety of spatiotemporal phenomena [11,12], such as oscillatory Turing patterns, standing wave labyrinths, rotating spirals, and mixed mode oscillations [13] resulting in spatiotemporal chaos and intermittency. These developments have been the subject of a large body of literature [14] over the past couple of decades.

To put the present work in an appropriate perspective we begin by distinguishing two different situations of periodic forcing. First, when the system is directly driven [15], the forced oscillation occurs for any strength of forcing. Second, when the parameter of a system, say a frequency is driven, the system undergoes sustained periodic oscillation [16] at a subharmonic frequency with respect to the forcing frequency provided the strength of periodic forcing is raised beyond a critical instability threshold. In the present paper we deal with the second situation in the context of oscillatory chemical reaction and reaction-diffusion systems. Parametric instability [17] was investigated earlier in several areas of physical sciences, e.g., in ruffled surface waves in hydrodynamics [18], in mechanical vibrations [19], in tuning organ pipes in acoustics [20], for exciting oscillators in electrical circuits [21], for wave-mixing and wave amplification using nonlinear crystals

in optics [22], and in nonlinear active devices like Josephson junctions [23]. In the context of chemical reactions [24] a single chemical oscillator in the steady state was demonstrated to exhibit parametric oscillation by suitably modulating a scaling parameter at twice the oscillation frequency beyond a critical pumping strength. In presence of diffusion [25] the single system under this condition can exhibit spatiotemporal profiles, stationary in space but periodic in time. These profiles appear as standing clusters observed in experiments [26]. Our focus in this paper lies on parametric instability in diffusively coupled oscillatory chemical reactions [27–29] and coupled reaction-diffusion systems [29–37]. Coupling of excitable and oscillatory chemical systems and reaction-diffusion systems between thin layers through transverse diffusivity and nonlinearity are well known for quite sometime in several other contexts. The examples include, among others, generation of wave instability [30] yielding twinkling eye patterns and stationary Turing patterns, use of Kuramoto-like nonlocal coupled chemical oscillators to generate chimera states consisting of coexisting subpopulations of synchronized and unsynchronized oscillators [27], formation of self-organized pacemakers using coupled reaction-diffusion systems [31], lattice gas automata model for coupled reaction-diffusion systems [32], use of diffusively coupled BZ oscillators with global feedback to generate in-phase and antiphase oscillations [33], and phase-lag synchronization in networks of photochemically coupled chemical oscillators with a broad frequency distribution [28]. Chaotic instability and various bifurcation scenarios have been analyzed in coupled BZ systems [29] and in coupled reaction-diffusion systems [34], respectively. It has also been demonstrated that coupling in excitable media may lead to spontaneously generated periodic wave [35] while spiral waves can be triggered by linear coupling of reaction-diffusion systems [36]. Turing pattern formation has been studied also in coupled reaction-diffusion systems with distributed delays [37]. Our objective in this paper is to demonstrate how the diffusive coupling between two lay-

^{*}Corresponding author: pcdsr@iacs.res.in

ers can induce temporal or spatiotemporal synchronization in oscillatory chemical reaction or reaction-diffusion systems through parametric instability. We consider a model of chemical reaction with and without diffusion in two layers which are transversely coupled minimally and one of the components in one layer is parametrically driven by a sinusoidal time-varying force. It has been shown that when the forcing frequency matches twice the oscillation frequency, the system in both layers undergoes sustained parametric temporal or spatiotemporal oscillations which gets synchronized, when the strength of forcing and strength of coupling are maintained beyond their critical instability thresholds. We have formulated a general scheme to derive the critical thresholds for coupling and forcing which determine the range of wavelength for this parametric instability and antiphase synchrony in temporal oscillations and spatiotemporal patterns. Our theoretical analysis is illustrated with the help of an activator-inhibitor model with Gierer-Meinhardt kinetics used widely in the context of developmental biology and full numerical simulations.

The outline of the paper is as follows: In Sec. II we have presented a general scheme of two-layer coupled oscillatory chemical system to derive the threshold conditions for parametric instability in the coupled system leading to synchronization of sustained oscillations. This is followed by detailed numerical simulation of Gierer-Meinhardt model for illustration. The scheme is extended to reaction-diffusion system in Sec. III. The conditions for parametric instability-induced spatiotemporal synchronization are worked out on the basis of a multiple timescale perturbation analysis. Numerical simulations have been carried out to demonstrate synchronized spatiotemporal pattern formation. The paper is concluded in Sec. IV.

II. PARAMETRIC INSTABILITY INDUCED SYNCHRONIZATION IN CHEMICAL OSCILLATION IN COUPLED CHEMICAL SYSTEM

A. General scheme

We begin by considering a general two-layer coupled oscillatory chemical system whose kinetics is given by the following equations:

$$\text{Primary layer } \begin{cases} \dot{u}_1 = f(u_1, v_1) + a \sin(\omega_p t) u_1 + \alpha(u_1 - u_2) \\ \dot{v}_1 = g(u_1, v_1) \end{cases}, \quad (2.1)$$

$$\text{Secondary layer } \begin{cases} \dot{u}_2 = f(u_2, v_2) + \alpha(u_2 - u_1) \\ \dot{v}_2 = g(u_2, v_2) \end{cases}, \quad (2.2)$$

where u_1 and v_1 refer to the concentration of the chemical species involved in primary layer and u_2 and v_2 are the concentration of the corresponding chemical species in the secondary layer; f and g are, in general, nonlinear functions. Two layers are transversely coupled through variables u_1 and u_2 with the coupling constant α in the spirit of inhibitor [35] or activator [36] coupled models. $a \sin(\omega_p t)$ is the sinusoidal parametric forcing term acting on u_1 in the primary layer where a and ω_p are the amplitude and frequency of the parametric forcing, respectively. The dynamical system has a

steady state at $(u_1^0, v_1^0, u_2^0, v_2^0)$ and linearization of the system around the steady state leads us to the time evolution of the small perturbation $(\delta u_1, \delta v_1, \delta u_2, \delta v_2)$ expressed as

$$\delta \dot{u}_1 = (f_{u_1} + a \sin(\omega_p t) + \alpha) \delta u_1 + f_{v_1} \delta v_1 - \alpha \delta u_2, \quad (2.3)$$

$$\delta \dot{v}_1 = g_{u_1} \delta u_1 + g_{v_1} \delta v_1, \quad (2.4)$$

$$\delta \dot{u}_2 = -\alpha \delta u_1 + (f_{u_2} + \alpha) \delta u_2 + f_{v_2} \delta v_2, \quad (2.5)$$

$$\delta \dot{v}_2 = g_{u_2} \delta u_2 + g_{v_2} \delta v_2, \quad (2.6)$$

where $f_{u_i}, f_{v_i}, g_{u_i}, g_{v_i}$ are the usual first derivatives of the functions f and g with respect to u_i and v_i as the subscripts indicate. Here the index i is 1 or 2 for the primary and secondary layers, respectively. The conditions $(f_{u_i} + g_{v_i}) < 0$ and $(f_{u_i} g_{v_i} - f_{v_i} g_{u_i}) > 0$ ensure the stability of the steady states (u_1^0, v_1^0) and (u_2^0, v_2^0) of the uncoupled oscillators. By differentiating Eq. (2.4) and Eq. (2.6) with respect to time t and manoeuvring the resulting equations using the relations of Eqs. (2.3)–(2.6), one can write

$$\begin{aligned} \delta \ddot{v}_1 + [\gamma_1 - \alpha - a \sin(\omega_p t)] \delta \dot{v}_1 \\ + [\Omega_1^2 + g_{v_1} \{\alpha + a \sin(\omega_p t)\}] \delta v_1 + (\alpha \beta) \delta \dot{v}_2 \\ - (\alpha \beta g_{v_2}) \delta v_2 = 0, \end{aligned} \quad (2.7)$$

$$\begin{aligned} \delta \ddot{v}_2 + [\gamma_2 - \alpha] \delta \dot{v}_2 + [\Omega_2^2 + \alpha g_{v_2}] \delta v_2 + \left(\frac{\alpha}{\beta}\right) \delta \dot{v}_1 \\ - \left(\frac{\alpha g_{v_1}}{\beta}\right) \delta v_1 = 0, \end{aligned} \quad (2.8)$$

$$\text{where } \gamma_i = -(f_{u_i} + g_{v_i}); \Omega_i^2 = (f_{u_i} g_{v_i} - f_{v_i} g_{u_i}).$$

As per the conditions of steady state, γ_i and Ω_i^2 are both positive. Equation (2.7) and Eq. (2.8) therefore describe the linear primary and secondary oscillators, respectively. As expected the characteristic frequency and the damping constant of each oscillator get affected by the coupling constant α . The characteristic frequency of the primary oscillator on the other hand is modulated parametrically by an external time-dependent part $\sin(\omega_p t)$. In absence of the parametric forcing and the coupling terms the oscillators reduce to their usual damped harmonic form:

$$\delta \ddot{v}_i + \gamma_i \delta \dot{v}_i + \Omega_i^2 \delta v_i = 0; \text{ with } i = 1, 2. \quad (2.9)$$

The distinct feature of the primary oscillator described by the Eq. (2.7) is that it is capable of parametric oscillation. It is expected that because of the coupling terms in Eqs. (2.7) and (2.8) this may induce sustained periodic oscillation to the secondary oscillator resulting in synchronization [38]. To explore this scenario we assume solutions

$$\delta v_1(t) = x_1 \cos(\omega t), \quad (2.10)$$

$$\delta v_2(t) = x_2 \cos(\omega t), \quad (2.11)$$

for periodic oscillations at a frequency ω , where x_1 and x_2 are the amplitude of the signal wave of the primary and secondary oscillators, respectively. Expanding $\sin(\omega_p t)$ in Eq. (2.7) in terms of exponentials and substituting Eq. (2.10) and (2.11), we write

$$\left(\left[\left[-\frac{\omega^2}{2} + \frac{(\Omega_1^2 + \alpha g_{v_1})}{2} \right] + \left[\frac{(\gamma_1 - \alpha)\omega}{2} \right] i \right) e^{i\omega t} + \left\{ \left(\frac{a\omega}{4} \right) + \left(\frac{\alpha g_{v_1}}{4} \right) i \right\} e^{i(\omega_p - \omega)t} \right) x_1 + \left[\left\{ \left(-\frac{\alpha \beta g_{v_2}}{2} \right) + \left(\frac{\alpha \beta \omega}{2} \right) i \right\} e^{i\omega t} \right] x_2 = 0 \tag{2.12}$$

and

$$\left(\left[\left[-\frac{\omega^2}{2} + \frac{(\Omega_2^2 + \alpha g_{v_2})}{2} \right] + \left[\frac{(\gamma_2 - \alpha)\omega}{2} \right] i \right) e^{i\omega t} \right) x_2 + \left[\left\{ \left(-\frac{\alpha g_{v_1}}{2\beta} \right) + \left(\frac{\alpha \omega}{2\beta} \right) i \right\} e^{i\omega t} \right] x_1 = 0. \tag{2.13}$$

In deriving the above equation we have discarded all the nonsynchronous terms. From Eq. (2.12) it follows that sustained oscillation is possible if

$$\omega_p - \omega = \omega ; \text{ or, } \omega_p = 2\omega. \tag{2.14}$$

This is the condition for parametric resonance. From Eqs. (2.12)–(2.14) one obtains

$$\frac{x_1}{x_2} = \frac{\left\{ \left(\frac{\alpha \beta g_{v_2}}{2} \right) - \left(\frac{\alpha \beta \omega}{2} \right) i \right\}}{\left\{ \left[-\frac{\omega^2}{2} + \frac{(\Omega_1^2 + \alpha g_{v_1})}{2} + \frac{a\omega}{4} \right] + \left[\frac{(\gamma_1 - \alpha)\omega}{2} + \frac{\alpha g_{v_1}}{4} \right] i \right\}}, \tag{2.15}$$

$$\text{and } \frac{x_1}{x_2} = \frac{\left\{ \left[-\frac{\omega^2}{2} + \frac{(\Omega_2^2 + \alpha g_{v_2})}{2} \right] + \left[\frac{(\gamma_2 - \alpha)\omega}{2} \right] i \right\}}{\left\{ \left(\frac{\alpha g_{v_1}}{2\beta} \right) - \left(\frac{\alpha \omega}{2\beta} \right) i \right\}}, \tag{2.16}$$

use of the above two equations yields

$$\begin{aligned} [(\Omega_2^2 - \omega^2) + \alpha g_{v_2}] [(\Omega_1^2 - \omega^2) + \alpha g_{v_1} + \frac{a\omega}{2}] - [(\gamma_2 - \alpha)\omega] \left[(\gamma_1 - \alpha)\omega + \frac{\alpha g_{v_1}}{2} \right] \\ = \alpha^2 (g_{v_1} g_{v_2} - \omega^2), \end{aligned} \tag{2.17}$$

$$\begin{aligned} [\omega(\gamma_2 - \alpha)] \left[(\Omega_1^2 - \omega^2) + \alpha g_{v_1} + \frac{a\omega}{2} \right] + \left[\omega(\gamma_1 - \alpha) + \frac{\alpha g_{v_1}}{2} \right] [(\Omega_2^2 - \omega^2) + \alpha g_{v_2}] \\ = \alpha^2 \omega (g_{v_1} + g_{v_2}). \end{aligned} \tag{2.18}$$

Equations (2.17) and (2.18) can be solved to obtain critical forcing strength a as

$$a = \frac{2[\gamma_1 \gamma_2 \omega^2 - \alpha(\gamma_1 + \gamma_2)\omega^2 - \Delta_1 \Delta_2 - \alpha(\Delta_1 g_{v_2} + \Delta_2 g_{v_1})]}{[\omega \Delta_2 - \omega g_{v_1} \gamma_2 + \alpha(g_{v_1} + g_{v_2})\omega]}, \tag{2.19}$$

where the coupling strength α is given as an appropriate solution of the following cubic equation:

$$P_1 \alpha^3 + P_2 \alpha^2 + P_3 \alpha + P_4 = 0, \tag{2.20}$$

where

$$\begin{cases} P_1 = [2\omega^2(g_{v_1} + g_{v_2})^2] \\ P_2 = \{ [2\omega^2(g_{v_1} + g_{v_2})(\Delta_2 - g_{v_1} \gamma_2)] + [g_{v_1} g_{v_2} - \omega^2][\omega^2(\gamma_1 + \gamma_2) + (g_{v_1} \Delta_2 + g_{v_2} \Delta_1)] \} \\ \quad - \{ \omega^2(g_{v_1} + g_{v_2})(g_{v_1} \gamma_2 + g_{v_2} \gamma_1 - \Delta_1 - \Delta_2) \} \\ P_3 = -\{ [\omega^2(\Delta_2 - g_{v_1} \gamma_2)(g_{v_1} \gamma_2 + g_{v_2} \gamma_1 - \Delta_1 - \Delta_2)] + \{ (g_{v_1} g_{v_2} - \omega^2)(\gamma_1 \gamma_2 \omega^2 - \Delta_1 \Delta_2) \} \} \\ \quad - \{ (\omega^2 \gamma_2 + g_{v_1} \Delta_2)[(\gamma_1 + \gamma_2)\omega^2 + (g_{v_1} \Delta_2 + g_{v_2} \Delta_1)] \} + \{ \omega^2(\gamma_2 \Delta_1 + \gamma_1 \Delta_2)(g_{v_1} + g_{v_2}) \} \\ P_4 = -\{ \omega^2(\gamma_2 \Delta_1 + \gamma_1 \Delta_2)(\Delta_2 - g_{v_1} \gamma_2) \} + \{ (\gamma_1 \gamma_2 \omega^2 - \Delta_1 \Delta_2)(\omega^2 \gamma_2 + g_{v_1} \Delta_2) \} \\ \Delta_i = (\Omega_i^2 - \omega^2); i = 1, 2. \end{cases}$$

The solution of Eqs. (2.19) and (2.20) gives us the critical values of coupling constant (α_c) and forcing strength (a_c). To evaluate α_c and a_c we first solve the cubic equation of coupling constant α , i.e., Eq. (2.20) using Newton-Raphson

iterative method and use the solution α_c to estimate the value of critical forcing strength a_c . The solution (α_c, a_c) represents the threshold condition for the sustained parametric synchronized oscillation of the coupled chemical

system. Summarizing the above discussions we note that the conditions for parametric instability leading to sustained synchronized chemical oscillation in the two layers are twofold; first, the condition for parametric resonance $\omega_p = 2\omega$ and second, the critical instability threshold condition on forcing strength a and on coupling strength α to overcome the dissipative effect of the dynamics. To corroborate the general scheme for the two-layer oscillatory chemical system we now consider a prototypical model of Gierer-Meinhardt kinetics [39,40] widely studied over the years as a testing ground for various theories of nonlinear chemical dynamics. The results of full numerical solutions are described in the subsequent sections.

B. Application and Gierer-Meinhardt kinetics

In order to corroborate our theoretical findings of the preceding subsection we now carry out detailed numerical simulation of the kinetic Gierer-Meinhardt model. The model consists of kinetic terms and diffusion terms. To validate our scheme we first take the kinetic terms into consideration which constitutes an activator-inhibitor dynamics. The equations describing the kinetic model that includes parametric driving as well as the coupling are as follows:

Primary oscillator

$$\begin{cases} \frac{\partial u_1}{\partial t} = \frac{u_1^2}{v_1} - u_1[1 - a \sin(\omega_p t)] + \phi_1 + \alpha(u_1 - u_2) \\ \frac{\partial v_1}{\partial t} = \mu_1(u_1^2 - v_1) \end{cases}, \quad (2.21)$$

Secondary oscillator

$$\begin{cases} \frac{\partial u_2}{\partial t} = \frac{u_2^2}{v_2} - u_2 + \phi_2 + \alpha(u_2 - u_1) \\ \frac{\partial v_2}{\partial t} = \mu_2(u_2^2 - v_2) \end{cases}. \quad (2.22)$$

Here u_i represents the activator concentration and v_i refers to the inhibitor concentration; ϕ_i and μ_i are the basic production rate and the relative removal rate, respectively. The homogeneous steady state of the uncoupled system is given as $u_i^0 = (1 + \phi_i)$ and $v_i^0 = (1 + \phi_i)^2$, for $i = 1, 2$. Although this kinetic model is a two parameter system, the steady state depends only on one parameter ϕ_i but not on μ_i . For the steady state of the coupled system one must choose the parameter $\phi_1 = \phi_2$. It follows from the linear stability analysis of the uncoupled system that Hopf bifurcation curve is given by

$$\mu_H = \frac{1 - \phi_i}{1 + \phi_i}. \quad (2.23)$$

The Hopf bifurcation is illustrated by the solid red line in Fig. 1. The stripped gray region under the curve portrays the homogeneous oscillatory state and the white region above the curve represents the homogeneous stable state. For the present purpose we choose the steady state for the primary as well as secondary oscillator located at the homogeneous stable (white) region of Fig. 1, for the parameter set $\mu_1 = 0.35$, $\phi_1 = 0.6$, $\mu_2 = 0.35$, and $\phi_2 = 0.5$. The coupled system in the region does not remain in the steady state and furthermore

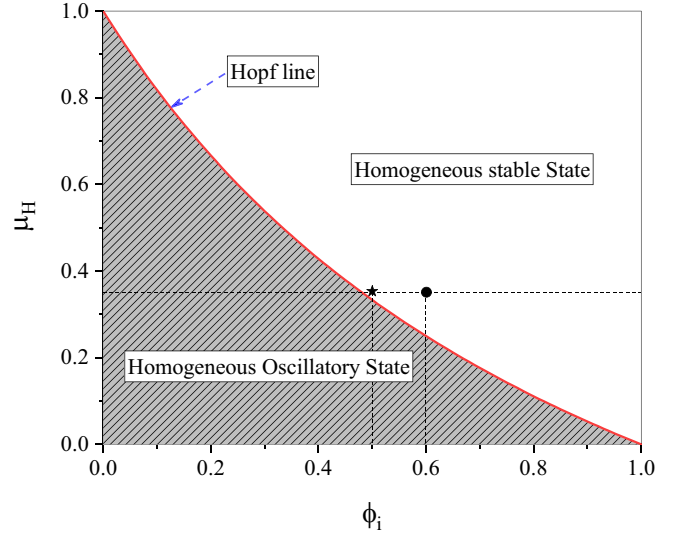


FIG. 1. μ_H vs. ϕ plot of Hopf bifurcation curve for the uncoupled system. The points marked by star and dot correspond to two different steady states of the uncoupled system (units arbitrary).

by virtue of Eqs. (2.19) and (2.20) the given parameter set yields the values of critical coupling constant $\alpha_c = 0.0345$ and critical forcing strength $a_c = 0.1524$. Having known the bifurcation diagram and the critical instability thresholds for coupling and the forcing strength Eqs. (2.22) and (2.23) are numerically solved using the fourth-order Runge-Kutta method with time step $\Delta t = 0.01$.

The results of the numerical simulations are presented in the Figs. 2 and 3 for the coupled dynamics below and above the instability threshold, respectively. When the forcing strength a and the coupling strength α are set below their threshold values, the oscillation of concentration of activator in the primary as well as in the secondary layer takes place at a forcing frequency as shown in Fig. 2(a). Furthermore the long time waveform shows that the oscillation is accompanied by damping and continuous without synchronization. The phase diagrams depicting the stable and parametrically unstable regions in terms of a - μ plot and α - μ plot are shown in Figs. 2(b) and 2(c), respectively. These two plots are the two-dimensional projections of the surface defined by a , μ , and α . The chosen points in the plots are shown for the values $\mu = 0.35$, $a = 0.1024$, and $\alpha = 0.0145$ which correspond to the region below the parametric instability threshold. For higher values of a and α beyond their critical instability thresholds characterized by $a_c = 0.1524$ and $\alpha_c = 0.0345$, the coupled system exhibits sustained synchronized parametric oscillation at $\omega = \frac{\omega_p}{2}$, i.e., at half the forcing frequency. This is shown in Fig. 3(a). The phase diagrams are shown in Figs. 3(b) and 3(c) for the parameter set corresponding to the threshold values α_c , a_c , and μ_c , for synchronized parametric oscillation. Two uncoupled chemical oscillators in two layers in different steady states can thus be coupled and subjected to a parametric forcing beyond the critical threshold values of coupling and forcing strength to excite synchronized sustained oscillation at a subharmonic frequency. It is easy to check that the oscillations in the two layers are in antiphase disposition.

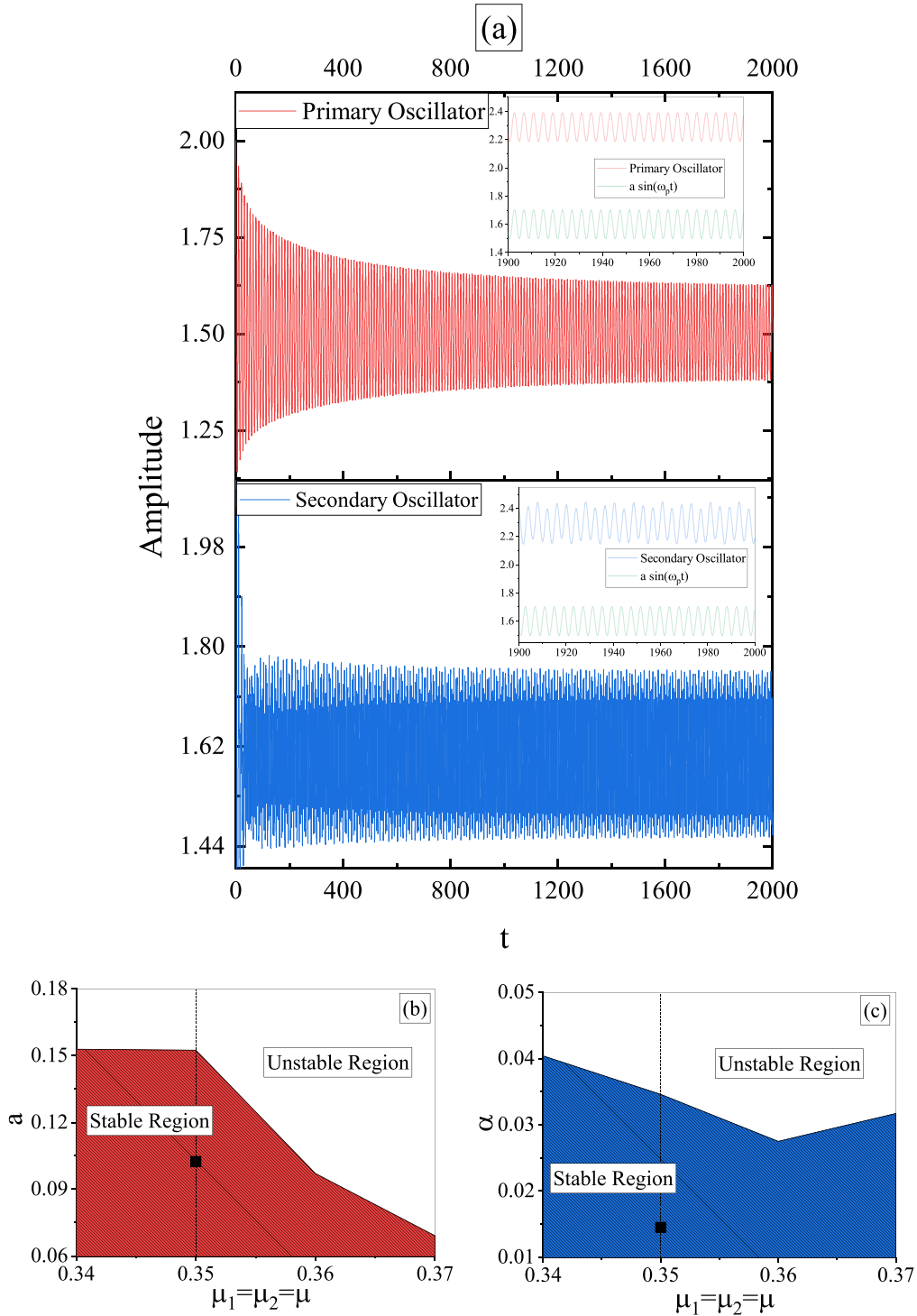


FIG. 2. (a) Forced unsynchronized oscillation of the coupled system: Temporal profile of oscillatory concentration (u_1) of primary layer (plotted with red line) and concentration (u_2) of secondary layer (plotted with blue line) below the critical values of coupling constant $\alpha_c = 0.1524$ and forcing strength $a_c = 0.0345$ for the parameter set $\phi_1 = 0.6, \mu_1 = 0.35, \phi_2 = 0.5, \mu_2 = 0.35, \omega_p = 1.143$ and for $a = 0.1024, \alpha = 0.0145$. The green oscillatory lower profile of the inset plot represents parametric forcing $a \sin(\omega_p t)$ and is shown for comparison with the concentration profile oscillatory at ω_p over a short time window. (b) Phase diagram (explained in the text) on the μ - a plane where the white region represents the unstable region, i.e., the region of parametric oscillation and the red region represents the stable region, i.e., the region of forced oscillation along with the chosen point $\mu = 0.35, a = 0.1024$. (c) Phase diagram (explained in the text) on the μ - α plane where the white region represents the unstable region, i.e., the region of parametric oscillation and the blue region represents the stable region, i.e., the region of forced oscillation along with the chosen point $\mu = 0.35, \alpha = 0.0145$ (units arbitrary).

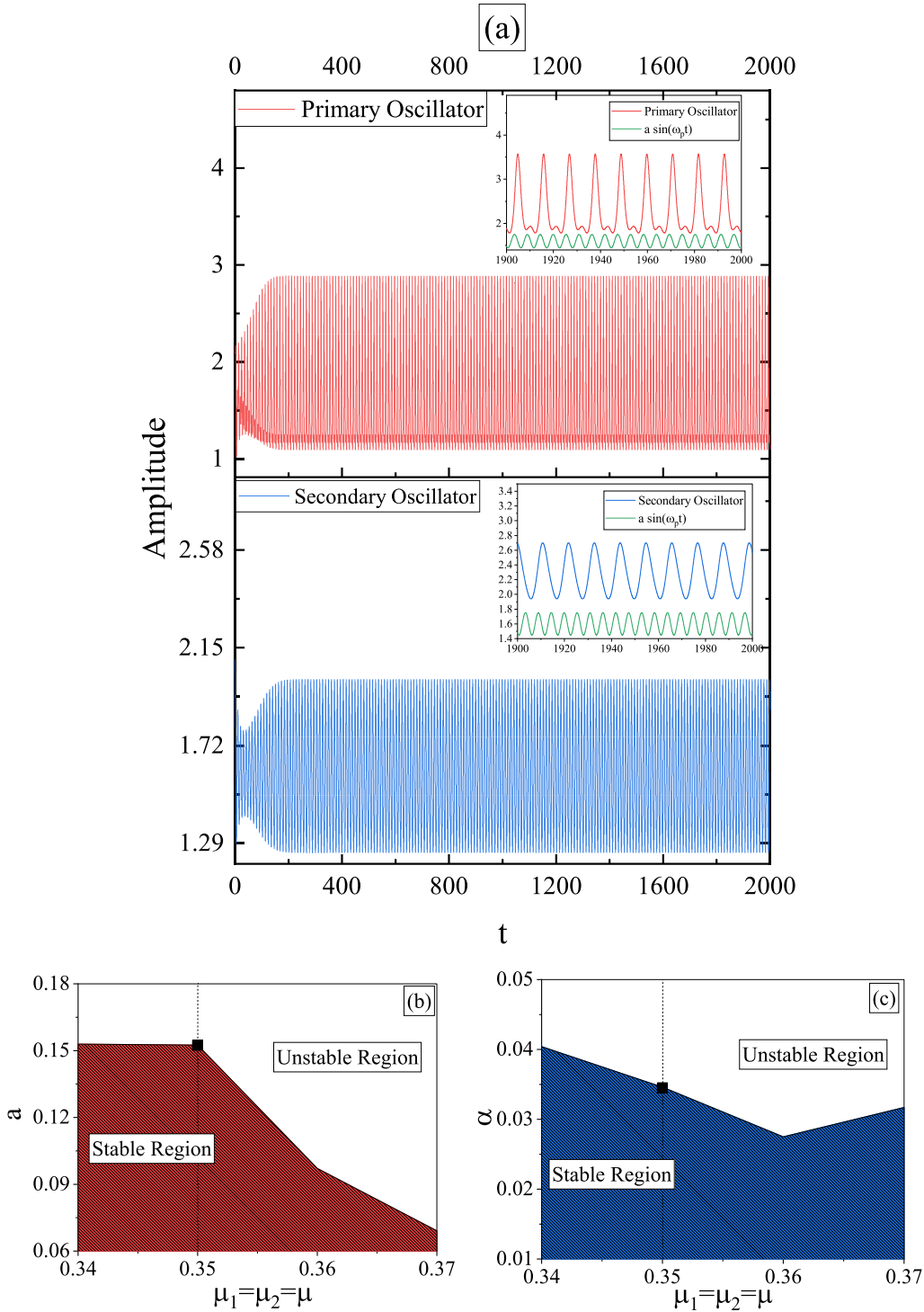


FIG. 3. (a) Temporal antiphase synchronization of oscillation at $\frac{\omega_p}{2}$ under parametric forcing: Profile of oscillatory concentration (u_1) of primary layer (plotted with red line) and concentration (u_2) of secondary layer (plotted with blue line) at the critical values of coupling constant $\alpha_c = 0.1524$ and forcing strength $a_c = 0.0345$ for the parameter set $\phi_1 = 0.6$, $\mu_1 = 0.35$, $\phi_2 = 0.5$, $\mu_2 = 0.35$, $\omega_p = 1.143$, and for $a = 0.1524$, $\alpha = 0.0345$. The green oscillatory lower profile of the inset plot represents parametric forcing, $a \sin(\omega_p t)$ and is shown for comparison with concentration profile oscillations at $\frac{\omega_p}{2}$ over a shorter time window. The phase diagrams (b) and (c) are same as in Figs. 2(b) and 2(c) but for the parameter set mentioned above. The chosen point denoted by dark squares lies at the boundary between the stable and parametrically unstable regions (units arbitrary).

III. SPATIOTEMPORAL SYNCHRONIZATION IN COUPLED REACTION-DIFFUSION SYSTEMS

A. General considerations and inclusion of diffusion

To start with we consider a pair of coupled reaction-diffusion systems in two variables, u and v . The dynamical equations in two dimensions (x, y) can be written down as follows:

Primary layer

$$\begin{cases} \dot{u}_1 = f(u_1, v_1) + a \sin(\omega_p t) u_1 + \alpha(u_1 - u_2) + D_1 \nabla^2 u_1 \\ \dot{v}_1 = g(u_1, v_1) + \nabla^2 v_1 \end{cases}, \quad (3.1)$$

$$\text{Secondary layer} \quad \begin{cases} \dot{u}_2 = f(u_2, v_2) + \alpha(u_2 - u_1) + D_2 \nabla^2 u_2 \\ \dot{v}_2 = g(u_2, v_2) + \nabla^2 v_2 \end{cases}. \quad (3.2)$$

Here $u_i(x, y, t)$ and $v_i(x, y, t)$ are the concentration of the two reacting species; D_i represents the ratio of the diffusion coefficients of the chemical species participating in the reaction, i.e., $D_i = \frac{D_{u_i}}{D_{v_i}}$, with $i = 1$ and $i = 2$ denoting the primary and secondary layers, respectively. f and g are, in general, nonlinear kinetic terms. Two layers are transversely coupled through diffusion as in the previous section. Linearization of the system around the steady state leads us to the time evolution of the small spatiotemporal perturbation $(\delta u_1, \delta v_1, \delta u_2, \delta v_2)$ expressed as

$$\delta \dot{u}_1 = [f_{u_1} + D_1 \nabla^2 + a \sin(\omega_p t) + \alpha] \delta u_1 + f_{v_1} \delta v_1 - \alpha \delta u_2, \quad (3.3)$$

$$\delta \dot{v}_1 = g_{u_1} \delta u_1 + [g_{v_1} + \nabla^2] \delta v_1, \quad (3.4)$$

$$\delta \dot{u}_2 = -\alpha \delta u_1 + [f_{u_2} + D_2 \nabla^2 + \alpha] \delta u_2 + f_{v_2} \delta v_2, \quad (3.5)$$

$$\delta \dot{v}_2 = g_{u_2} \delta u_2 + [g_{v_2} + \nabla^2] \delta v_2. \quad (3.6)$$

Assuming spatiotemporal perturbations $\delta u_1, \delta v_1, \delta u_2, \delta v_2$ in two dimensions of the forms $\delta u_i = \delta U_i(t) \cos(K_x x + K_y y)$ and $\delta v_i = \delta V_i(t) \cos(K_x x + K_y y)$, $i = 1, 2$ and using them in Eqs. (3.3)–(3.6) yields the following set of kinetic equations:

$$\delta \dot{U}_1 = [f'_{u_1} + a \sin(\omega_p t) + \alpha] \delta U_1 + f_{v_1} \delta V_1 - \alpha \delta U_2, \quad (3.7)$$

$$\delta \dot{V}_1 = g_{u_1} \delta U_1 + [g'_{v_1}] \delta V_1, \quad (3.8)$$

$$\delta \dot{U}_2 = -\alpha \delta U_1 + [f'_{u_2} + \alpha] \delta U_2 + f_{v_2} \delta V_2, \quad (3.9)$$

$$\delta \dot{V}_2 = g_{u_2} \delta U_2 + [g'_{v_2}] \delta V_2, \quad (3.10)$$

where

$$f'_{u_i} = f_{u_i} - D_i(K_x^2 + K_y^2)$$

$$g'_{v_i} = g_{v_i} - (K_x^2 + K_y^2); \text{ with } i = 1, 2.$$

As in the preceding section, Eqs. (3.7)–(3.10) can be rewritten in the form of two second-order coupled ordinary differential

equations for the two layers,

$$\begin{aligned} \delta \ddot{V}_1 + [\gamma_1 - \alpha - a \sin(\omega_p t)] \delta \dot{V}_1 \\ + [\Omega_1^2 + g'_{v_1} \{\alpha + a \sin(\omega_p t)\}] \delta V_1 \\ + \alpha \beta \delta \dot{V}_2 - \alpha \beta g'_{v_2} \delta V_2 = 0, \end{aligned} \quad (3.11)$$

$$\begin{aligned} \delta \ddot{V}_2 + [\gamma_2 - \alpha] \delta \dot{V}_2 + [\Omega_2^2 + g'_{v_2} \alpha] \delta V_2 \\ + \frac{\alpha}{\beta} \delta \dot{V}_1 - \frac{\alpha}{\beta} \beta g'_{v_1} \delta V_1 = 0, \end{aligned} \quad (3.12)$$

where we have defined

$$\gamma_i = -(f'_{u_i} + g'_{v_i}) = -[f_{u_i} + g_{v_i} - (D_i + 1)K^2];$$

$$K^2 = K_x^2 + K_y^2; \beta = \frac{g_{u_1}}{g_{u_2}}$$

$$\begin{aligned} \Omega_i^2 = (f'_{u_i} g'_{v_i} - f_{v_i} g_{u_i}) = [D_i K^4 - \{f_{u_i} + g_{v_i} D_i\} K^2 \\ + \{f_{u_i} g_{v_i} - f_{v_i} g_{u_i}\}]; \quad i = 1, 2. \end{aligned}$$

Equations (3.11) and (3.12) are the starting point of our analysis for spatiotemporal synchronization induced by parametric driving of the reaction-diffusion system.

B. Parametric spatiotemporal instability and synchronization: A multiscale analysis

Having formulated the general scheme of parametrically driven coupled reaction-diffusion systems as governed by Eqs. (3.11) and (3.12) we now resort to an analysis of stability boundaries of the coupled system. Our objective here to locate the regions where the primary layer loses its stability with the emergence of pattern forming solutions with growing normal modes. The dynamical Eqs. (3.11) and (3.12) can be rewritten in a modified timescale $\tau = \omega_p t$ as follows:

$$\begin{aligned} \delta \ddot{V}_1 + \epsilon \rho_1 [1 - c_1 \sin(\tau)] \delta \dot{V}_1 + \left[v_1 + g'_{v_1} \left(\frac{\alpha}{a} + \sin \tau \right) \right] \delta V_1 \\ + [\sigma \omega_p] \epsilon \delta \dot{V}_2 - [\sigma g'_{v_2}] \epsilon \delta V_2 = 0, \end{aligned} \quad (3.13)$$

$$\begin{aligned} \delta \ddot{V}_2 + \epsilon \rho_2 \delta \dot{V}_2 + \left[v_2 + \left(\frac{\alpha g'_{v_2}}{a} \right) \epsilon \right] \delta V_2 \\ + [\sigma' \omega_p] \epsilon \delta \dot{V}_1 - [\sigma' g'_{v_1}] \epsilon \delta V_1 = 0, \end{aligned} \quad (3.14)$$

where $\epsilon = \frac{a}{\omega_p^2}$; $\kappa_i = (\gamma_i - \alpha)$; $\rho_i = \frac{\kappa_i \omega_p}{a}$; $c_1 = \frac{a}{\kappa_1}$; $v_i = \frac{\Omega_i^2}{\omega_p^2}$;

$$\sigma = \frac{\alpha \beta}{a}; \sigma' = \frac{\alpha}{\beta a}.$$

Equations (3.13) and (3.14) incorporate two timescales for small values of ϵ , the scaled forcing amplitude; the timescale $\xi = \tau$ corresponds to the periodic motion itself, and a slower timescale $\eta = \epsilon \tau$ represents the approach to the periodic motion. Expanding $\delta V_i(\xi, \eta)$ in a power series in ϵ as

$$\delta V_1(\xi, \eta) = \delta V_1^0(\xi) + \epsilon \delta V_1^1(\xi) + \epsilon^2 \delta V_1^2(\xi) + \dots, \quad (3.15)$$

$$\delta V_2(\xi, \eta) = \delta V_2^0(\xi) + \epsilon \delta V_2^1(\xi) + \epsilon^2 \delta V_2^2(\xi) + \dots, \quad (3.16)$$

in Eqs. (3.13) and (3.14), the resulting equations can be solved order by order. The zero-order equations are given by

$$\frac{\partial^2(\delta V_1^0)}{\partial \xi^2} + \nu_1 \delta V_1^0 = 0, \tag{3.17}$$

$$\frac{\partial^2(\delta V_2^0)}{\partial \xi^2} + \nu_2 \delta V_2^0 = 0, \tag{3.18}$$

which yield a set of solutions for simple harmonic oscillator with characteristic frequencies $\sqrt{\nu_1}$ and $\sqrt{\nu_2}$. We then write the slowly varying amplitude solutions as follows:

$$\delta V_1^0(\xi, \eta) = A_1(\eta) \cos(\sqrt{\nu_1}\xi) + B_1(\eta) \sin(\sqrt{\nu_1}\xi), \tag{3.19}$$

$$\delta V_2^0(\xi, \eta) = A_2(\eta) \cos(\sqrt{\nu_2}\xi) + B_2(\eta) \sin(\sqrt{\nu_2}\xi). \tag{3.20}$$

For the first order in ϵ and for the special choice $\nu_1 = \nu_2 = \frac{1}{4}$, we have

$$\begin{aligned} \frac{\partial^2(\delta V_1^1)}{\partial \xi^2} + \nu_1 \delta V_1^1 = & \left[\frac{\partial A_1}{\partial \eta} + \frac{\rho_1}{2} A_1 - \frac{\alpha g'_{v_1}}{a} B_1 + \frac{\rho_1 c_1}{4} B_1 - \frac{g'_{v_1}}{2} A_1 + \frac{\sigma \omega_p}{2} A_2 + (\sigma g'_{v_2}) B_2 \right] \sin \frac{\xi}{2} \\ & + \left[-\frac{\partial B_1}{\partial \eta} - \frac{\rho_1}{2} B_1 - \frac{\alpha g'_{v_1}}{a} A_1 - \frac{\rho_1 c_1}{4} A_1 - \frac{g'_{v_1}}{2} B_1 - \frac{\sigma \omega_p}{2} B_2 - (\sigma g'_{v_2}) A_2 \right] \cos \frac{\xi}{2} \\ & + \left[\frac{\rho_1 c_1}{4} B_1 - \frac{g'_{v_1}}{2} A_1 \right] \sin \frac{3\xi}{2} + \left[\frac{\rho_1 c_1}{4} A_1 - \frac{g'_{v_1}}{2} B_1 \right] \cos \frac{3\xi}{2}, \end{aligned} \tag{3.21}$$

$$\begin{aligned} \frac{\partial^2(\delta V_2^1)}{\partial \xi^2} + \nu_2 \delta V_2^1 = & \left[\frac{\partial A_2}{\partial \eta} + \frac{\rho_2}{2} A_2 - \frac{\alpha g'_{v_2}}{a} B_2 + \frac{\sigma' \omega_p}{2} A_1 + (\sigma' g'_{v_1}) B_1 \right] \sin \frac{\xi}{2} \\ & + \left[-\frac{\partial B_2}{\partial \eta} - \frac{\rho_2}{2} B_2 - \frac{\alpha g'_{v_2}}{a} A_2 - \frac{\sigma' \omega_p}{2} B_1 + (\sigma' g'_{v_1}) A_1 \right]. \end{aligned} \tag{3.22}$$

To avoid secular terms we set the coefficients of $\sin \frac{\xi}{2}$ and $\cos \frac{\xi}{2}$ equal to zero so that we have

$$\begin{pmatrix} \frac{\partial A_1}{\partial \eta} \\ \frac{\partial B_1}{\partial \eta} \\ \frac{\partial A_2}{\partial \eta} \\ \frac{\partial B_2}{\partial \eta} \end{pmatrix} = \begin{pmatrix} \frac{g'_{v_1} - \rho_1}{2} & \frac{\alpha g'_{v_1} - \rho_1 c_1}{a} & -\frac{\sigma \omega_p}{2} & -\sigma g'_{v_2} \\ -\frac{\alpha g'_{v_1} - \rho_1 c_1}{a} & \frac{\rho_1 + g'_{v_1}}{4} & -\sigma g'_{v_2} & -\frac{\sigma \omega_p}{2} \\ -\frac{\sigma' \omega_p}{2} & -\sigma' g'_{v_1} & -\frac{\rho_2}{2} & \frac{\alpha g'_{v_2}}{a} \\ \sigma' g'_{v_1} & -\frac{\sigma' \omega_p}{2} & -\frac{\alpha g'_{v_2}}{a} & -\frac{\rho_2}{2} \end{pmatrix} \begin{pmatrix} A_1 \\ B_1 \\ A_2 \\ B_2 \end{pmatrix}. \tag{3.23}$$

It is clear that A_1, B_1, A_2, B_2 have exponential growth. This instability arises because of $\nu_1 = \nu_2 = \frac{1}{4}$ and corresponds to a 2 : 1 subharmonic resonance in which the driving frequency (ω_p) is twice the natural frequency for each oscillator. Expanding ν_1 and ν_2 in a power series in ϵ one obtains

$$\nu_1 = \frac{1}{4} + \epsilon \nu_1^1 + \epsilon^2 \nu_1^2 + \dots, \tag{3.24}$$

$$\nu_2 = \frac{1}{4} + \epsilon \nu_2^1 + \epsilon^2 \nu_2^2 + \dots. \tag{3.25}$$

Repeating the same calculation with ν_1 and ν_2 we arrive at a set of coupled closed equations of A_1, B_1, A_2, B_2 which can be written in the following matrix representation:

$$\begin{pmatrix} \frac{\partial A_1}{\partial \eta} \\ \frac{\partial B_1}{\partial \eta} \\ \frac{\partial A_2}{\partial \eta} \\ \frac{\partial B_2}{\partial \eta} \end{pmatrix} = \begin{pmatrix} \frac{g'_{v_1} - \rho_1}{2} & \frac{\alpha g'_{v_1} - \rho_1 c_1}{a} + \nu_1^1 & -\frac{\sigma \omega_p}{2} & -\sigma g'_{v_2} \\ -\frac{\alpha g'_{v_1} - \rho_1 c_1}{a} + \nu_1^1 & \frac{\rho_1 + g'_{v_1}}{4} & -\sigma g'_{v_2} & -\frac{\sigma \omega_p}{2} \\ -\frac{\sigma' \omega_p}{2} & -\sigma' g'_{v_1} & -\frac{\rho_2}{2} & \frac{\alpha g'_{v_2}}{a} + \nu_2^1 \\ \sigma' g'_{v_1} & -\frac{\sigma' \omega_p}{2} & -\frac{\alpha g'_{v_2}}{a} + \nu_2^1 & -\frac{\rho_2}{2} \end{pmatrix} \begin{pmatrix} A_1 \\ B_1 \\ A_2 \\ B_2 \end{pmatrix}. \tag{3.26}$$

As both σ and σ' are proportional to the ratio $\frac{\alpha}{a}$ and the ratio is very small we can neglect the terms associated with σ and σ' to a leading order. This leads us to the following two equations:

$$\begin{pmatrix} \frac{\partial A_1}{\partial \eta} \\ \frac{\partial B_1}{\partial \eta} \end{pmatrix} = \begin{pmatrix} \frac{g'_{v_1} - \rho_1}{2} & \frac{\alpha g'_{v_1}}{a} - \frac{\rho_1 c_1}{4} + v_1^1 \\ -\frac{\alpha g'_{v_1}}{a} - \frac{\rho_1 c_1}{4} + v_1^1 & -\frac{\rho_1 + g'_{v_1}}{2} \end{pmatrix} \begin{pmatrix} A_1 \\ B_1 \end{pmatrix}, \tag{3.27}$$

$$\begin{pmatrix} \frac{\partial A_2}{\partial \eta} \\ \frac{\partial B_2}{\partial \eta} \end{pmatrix} = \begin{pmatrix} -\frac{\rho_2}{2} & \frac{\alpha g'_{v_2}}{a} + v_2^1 \\ -\frac{\alpha g'_{v_2}}{a} + v_2^1 & -\frac{\rho_2}{2} \end{pmatrix} \begin{pmatrix} A_2 \\ B_2 \end{pmatrix}. \tag{3.28}$$

As the main drive for instability in the system is the parametric forcing acting on the primary layer, the perturbative stability analysis of the primary layer is sufficient for locating the instability region. Therefore we consider the equation describing the primary layer, i.e., Eq. (3.27) and proceed further. The equation can be solved by assuming a solution in the form $A_1(\eta) = A_1^0 \exp(\eta\Lambda)$ and $B_1(\eta) = B_1^0 \exp(\eta\Lambda)$, for nontrivial constants A_1^0 and B_1^0 . The following condition must hold

$$\begin{vmatrix} \frac{g'_{v_1} - \rho_1}{2} - \Lambda & \frac{\alpha g'_{v_1}}{a} - \frac{\rho_1 c_1}{4} + v_1^1 \\ -\frac{\alpha g'_{v_1}}{a} - \frac{\rho_1 c_1}{4} + v_1^1 & -\frac{\rho_1 + g'_{v_1}}{2} - \Lambda \end{vmatrix} = 0. \tag{3.29}$$

The eigenvalues Λ_{\pm} are given by

$$\Lambda_{\pm} = -\frac{\rho_1}{2} \pm \frac{1}{2} \sqrt{g'_{v_1}{}^2 - 4 \left[v_1^1{}^2 + \left(\frac{2\alpha g'_{v_1}}{a} \right) v_1^1 + \left(\frac{\alpha g'_{v_1}}{a} \right)^2 - \left(\frac{\rho_1 c_1}{4} \right)^2 \right]}. \tag{3.30}$$

For the transition between stable and unstable regions, we set $\Lambda_{\pm} = 0$ and obtain

$$v_1^1 = -\left(\frac{\alpha g'_{v_1}}{a} \right) \pm \frac{1}{2} \sqrt{\left(\frac{\rho_1 c_1}{2} \right)^2 + g'_{v_1}{}^2 - \rho_1^2}. \tag{3.31}$$

v_1 is therefore modified to first order as follows:

$$v_1 = \frac{1}{4} - \epsilon \left(\frac{\alpha g'_{v_1}}{a} \right) \pm \frac{\epsilon}{2} \sqrt{\left(\frac{\rho_1 c_1}{2} \right)^2 + g'_{v_1}{}^2 - \rho_1^2}. \tag{3.32}$$

The above condition gives two transition curves emerging from $v_1 = \frac{1}{4}$ forming instability region inside a tilted **V**-shaped Arnold's-tongue profile in the ϵ - v_1 plane. For the outside region the system shows quasiperiodic motion. The spatial inhomogeneity or spatiotemporal patterns are likely to emerge in the instability origin of the tongue. The origin of tilt of the tongue is the diffusive coupling between the two layers through α . Keeping in mind that $\gamma_i, \kappa_i, \rho_i, c_1, v_i, \Omega_i$ depend on wavelength we find the dispersion relation in terms of ω_p as a function of K^2 from the relation $\frac{\Omega_i^2}{\omega_p^2} = \frac{1}{4}$ to obtain the allowed range of wavelength for specific choice of parametric frequency ω_p ,

$$\omega_p = \sqrt{4\{(f_{u_1} - DK^2)(g_{v_1} - K^2) - f_{v_1}g_{u_1}\}}, \tag{3.33}$$

for the given parameter values. In what follows we illustrate the general scheme of Arnold tongue and dispersion relation with the help of Gierer-Meinhardt reaction-diffusion system followed by detailed numerical simulations for pattern formation.

C. Application to Gierer-Meinhardt model: Parametric instability-induced synchronized spatiotemporal patterns

We now return to Gierer-Meinhardt kinetic model as discussed in Sec. **II B** and include the diffusion terms for the activator and inhibitor. The equations are described in a dimensionless form as follows:

$$\text{Primary layer} \begin{cases} \frac{\partial u_1}{\partial t} = \frac{u_1^2}{v_1} - u_1[1 - a \sin(\omega_p t)] + \phi_1 + \alpha(u_1 - u_2) + D_1 \nabla^2 u_1 \\ \frac{\partial v_1}{\partial t} = \mu_1(u_1^2 - v_1) + \nabla^2 v_1 \end{cases}, \tag{3.34}$$

$$\text{Secondary layer} \begin{cases} \frac{\partial u_2}{\partial t} = \frac{u_2^2}{v_2} - u_2 + \phi_2 + \alpha(u_2 - u_1) + D_2 \nabla^2 u_2 \\ \frac{\partial v_2}{\partial t} = \mu_2(u_2^2 - v_2) + \nabla^2 v_2 \end{cases}. \tag{3.35}$$

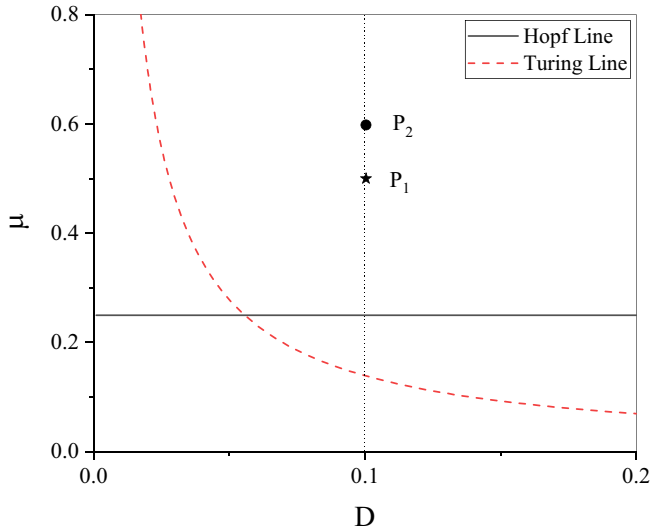


FIG. 4. Bifurcation diagram for the coupled Gierer-Meinhardt model without parametric forcing. The Hopf line (black solid line) and the Turing line (red dashed line) are shown in the μ - D parameter space for $\phi_1 = \phi_2 = \phi = 0.6$ and $D_1 = D_2 = D$ (units arbitrary). The points P_1 and P_2 are the chosen points in stable steady-state region for the primary and the secondary layers, respectively.

The homogeneous steady state of the uncoupled system is given in Sec. II B. Keeping note that they depend only on ϕ_i , we first choose $\phi_1 = \phi_2 (= \phi)$ for the rest of the treatment. Under this condition we have $u_1^0 = u_2^0$ and the linear stability analysis of the coupled reaction-diffusion system reveals the Hopf and Turing bifurcation lines which are given as $\mu_H = \frac{1-\phi_i}{1+\phi_i}$ and $\mu_T = \frac{1}{D}(\frac{2}{1+\phi} - 1)^2$, respectively. These bifurcation lines are shown in the μ - D plane in Fig. 4 for $\phi = 0.6$.

We now consider two points P_1 ($\mu_1 = 0.5$, $D_1 = 0.1$) and P_2 ($\mu_2 = 0.6$, $D_2 = 0.1$) in the stable steady-state region for $\phi_1 = \phi_2 = \phi = 0.6$ as shown in Fig. 4, for illustration of the analytical result obtained in the last section and numerical simulations. Using Eq. (3.33) we have plotted the dispersion relation ω_p vs. K^2 in Fig. 5 for the set of parameter values as mentioned earlier. It is evident that the choice of forcing frequency of the external sinusoidal field for parametric spatiotemporal oscillation and synchronization is not arbitrary but is dictated by the appropriate length scale of the spatially extended system.

Having determined the location of the two steady states P_1 and P_2 for the primary and secondary layers of the coupled system we now switch on parametric forcing term $a \sin(\omega_p t)$. The choice of ω_p , as shown in Fig. 5, is guided by K^2 . With $\omega_p = 1$ and $K^2 = 1$ and $\phi_1 = \phi_2 = \phi = 0.6$, $D_1 = D_2 = 0.1$, we set $\mu_1 = 0.5$ and $\mu_2 = 0.6$ corresponding to two points P_1 and P_2 and plot ϵ vs ν_1 using Eq. (3.32) for forcing strength $a = 0.5$ and coupling strength $\alpha = 0.5$. The result is presented in Fig. 6(a). A tilted Arnold's tongue appears in the ϵ - ν_1 parameter space separating out the gray unstable region in the middle of the tongue, from quasiperiodic stable region outside.

The linear stability analysis based on multiple timescale perturbation scheme as enumerated above is now corroborated

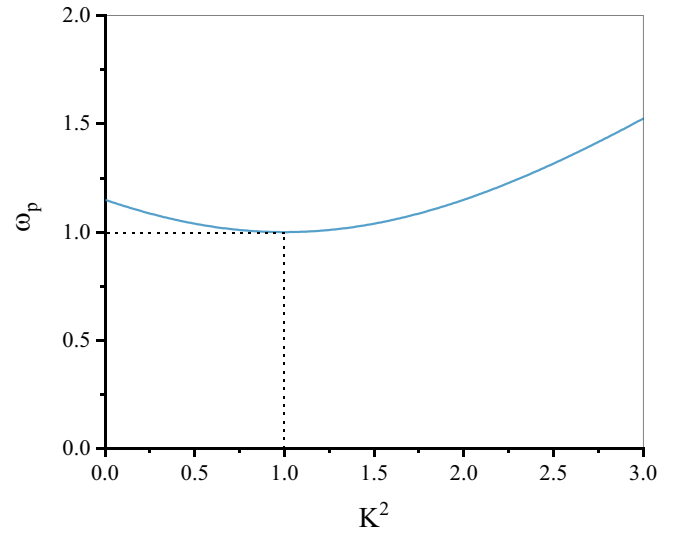


FIG. 5. The plot of dispersion relation [ω_p vs K^2 , Eq. (3.33)] for the set of parameters as mentioned in the text.

by a full scale numerical simulation of the coupled reaction-diffusion dynamics. To this end we return to Eqs. (3.34) and (3.35) and carry out numerical integration using Euler's algorithm over (250×250) discrete grid points in two dimensions for each of the two layers. The spatial resolution for the space coordinate and the time increment were set as $\Delta X = \Delta Y = 0.2$ and $\Delta t = 0.0025$, respectively. All the nodes of the grid were initially kept at the homogeneous steady state ($u_1^0 = u_2^0 = 1.6$ and $v_1^0 = v_2^0 = 2.56$). The system was perturbed by a weak random noise at grid point. The numerical integration was carried out using periodic boundary conditions over 5000 time units in each case. The results are plotted in Figs. 6(b) and 6(c) for the primary and the secondary layers, respectively at $t = 5000$ time units for a chosen parameter point $\gamma_1 = 0.4$, $\epsilon = 0.5$ [shown by star mark in stable quasiperiodic region, i.e., outside the tongue region in Fig. 6(a)]. As expected one observes uniform homogeneous spatiotemporal profiles for both the layers in complete agreement with our theoretical analysis.

As the coupling strength α is reduced to $\alpha = 0.3$ keeping the forcing strength same at $a = 0.5$, ϵ - ν_1 plot encompasses a larger unstable region inside the tongue as shown in Fig. 7(a). The star marked point at $\nu_1 = 0.4$ and $\epsilon = 0.5$ in ϵ - ν_1 parameter space now lies inside the tongue. We now proceed with numerical simulation of the coupled reaction-diffusion system. The development of the spatiotemporal profiles is depicted in Figs. 7(b)–7(d) and Figs. 7(e)–7(g) to 10 000 time units for the primary and secondary layers, respectively, at different time intervals. The parametric spatiotemporal instability leads to formation of patterns in the form of spots and stripes. It is interesting to note that the dark spots and stripes of the primary layer appear as bright spots and stripes of the secondary layer observed at the same time clearly indicating that they are synchronized with antiphase disposition. The patterns remain stationary in time. This is in sharp contrast to what one observes for parametric instability-induced pattern formation in single systems where the patterns in the form of

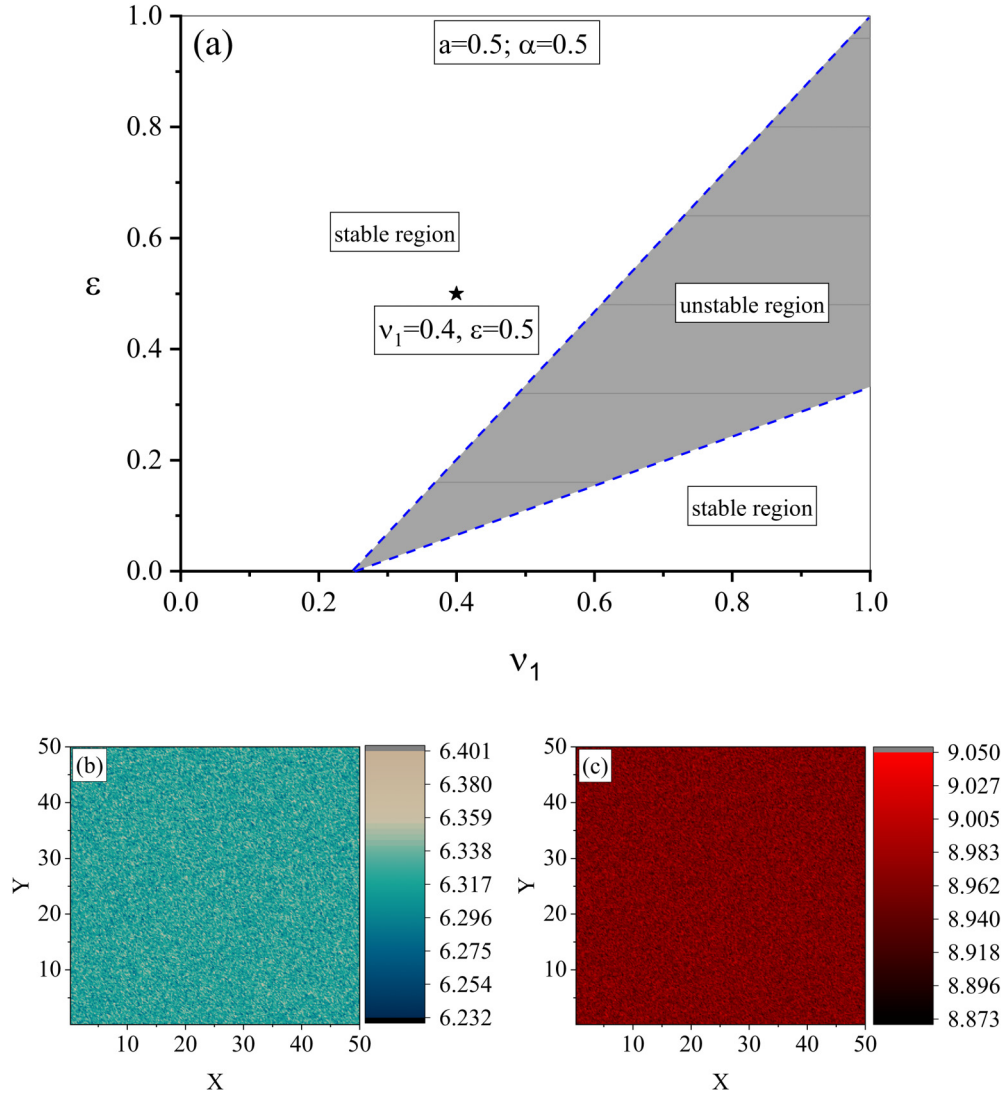


FIG. 6. (a) Tilted Arnold tongue in the $\epsilon - \nu_1$ plot [Eq. (3.32)] for the coupled Gierer-Meinhardt reaction-diffusion model for the two points $P_1 (\mu_1 = 0.5)$ and $P_2 (\mu_2 = 0.6)$ for $\phi_1 = \phi_2 = \phi = 0.6$ and $D_1 = D_2 = D = 0.1$ of Fig. 5 corresponding to stable steady-state region of the primary and the secondary layers and for $\omega_p = 1.0, K^2 = 1.0, a = 0.5, \alpha = 0.5$. The unstable region denoted by gray color inside the tongue while the outside region corresponds to stable quasiperiodic region; (b) spatiotemporal profiles of u_1 (primary layer) obtained by numerical simulation of parametrically driven Gierer-Meinhardt reaction-diffusion system [Eqs. (3.34) and (3.35)] at $t = 5000$ time units for $\nu_1 = 0.4$ and $\epsilon = 0.5$ and for other parameters as mentioned; (c) same as in (b) but for u_2 (secondary layer) (units arbitrary).

standing clusters remain oscillatory in time but stationary in space [25,26].

With further reduction of the value of coupling strength ($\alpha = 0.25$), the area of the unstable zone of the Arnold tongue in $\epsilon - \nu_1$ plot increases significantly. This is shown in Fig. 8(a). The star marked point $\nu_1 = 0.4$ and $\epsilon = 0.5$ still remains inside this region. We observe synchronized spatiotemporal patterns in the form of spots and stripes both for the primary and secondary layers corresponding to this point. The results are shown in Figs. 8(b)–8(d) and Figs. 8(e)–8(g).

We have further explored the effect of parametric forcing a and coupling constant α on the coupled reaction-diffusion system described by Eqs. (3.34) and (3.35) when the parameters of the system are chosen in such a way that the initial

state of system lies in the Turing region of the bifurcation diagram. To this end we have chosen $\mu_1 = \mu_2 = \mu = 0.4$ and the diffusion coefficients of the system $D_1 = D_2 = D = 0.03$. Figure 9(a) shows that the parameter set chosen for the simulation indeed lies in the Turing region of the bifurcation diagram. When we ran the simulation with $\alpha = 0.0$ and $a = 0.12$ the results depicted by Figs. 9(b) and 9(c) reveal that for this parameter set both layers are in the stationary spot-like patterned state as expected. We have also found that for lower values of the parametric forcing strength a the results remain qualitatively same as those shown in Figs. 9(b) and 9(c). When the parametric forcing strength is increased further, the primary layer, i.e., the layer which undergoes parametric forcing loses spatial heterogeneity, whereas the secondary layer

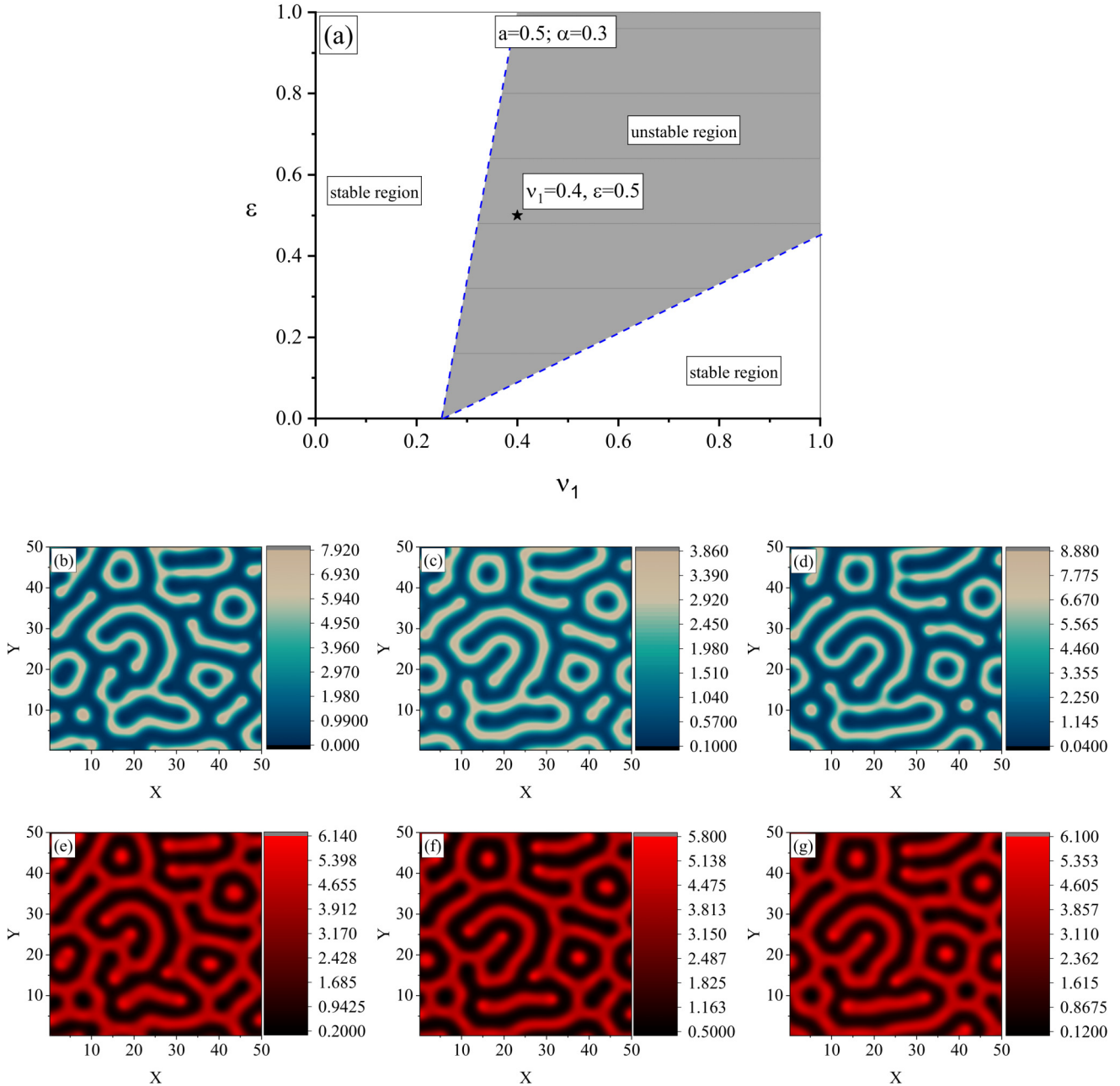


FIG. 7. (a) Same as in Fig. 6(a) but for $\alpha = 0.3$. [(b)–(d)] The spatiotemporal patterns obtained by numerical simulation of the coupled Gierer-Meinhardt reaction-diffusion system for the parameter set as mentioned in Fig. 6(a) for $v_1 = 0.4$ and $\epsilon = 0.5$ for u_1 (primary layer) at time (b) $t = 500$, (c) $t = 5000$, (d) $t = 10000$ time units; [(e)–(g)] same as in Figs. 7(b)–7(d) but for the secondary layer (units arbitrary).

remains as it is. This is shown in Figs. 9(d) and 9(e). Now under this situation if we raise the value of the coupling strength to $\alpha = 0.3$ the spotlike pattern reappear in the primary layer due to the propagation of instability from the secondary layer through coupling as shown in Figs. 9(f) and 9(g). Hence, we may conclude that the parametric forcing a plays a destructive role and coupling constant α plays a constructive role for the stationary patterns in coupled reaction-diffusion systems when the parameters are chosen in the Turing region of the

bifurcation diagram. The results are generically different from those observed earlier where the parameter set lies in the steady-state region.

Apart from the system described by Eqs. (3.34) and (3.35) there are other three possibilities regarding the presence of the parametric forcing term and the coupling term in the activator and inhibitor dynamics of the primary and secondary layers. In the rest of the section we discuss what happens to these three cases.

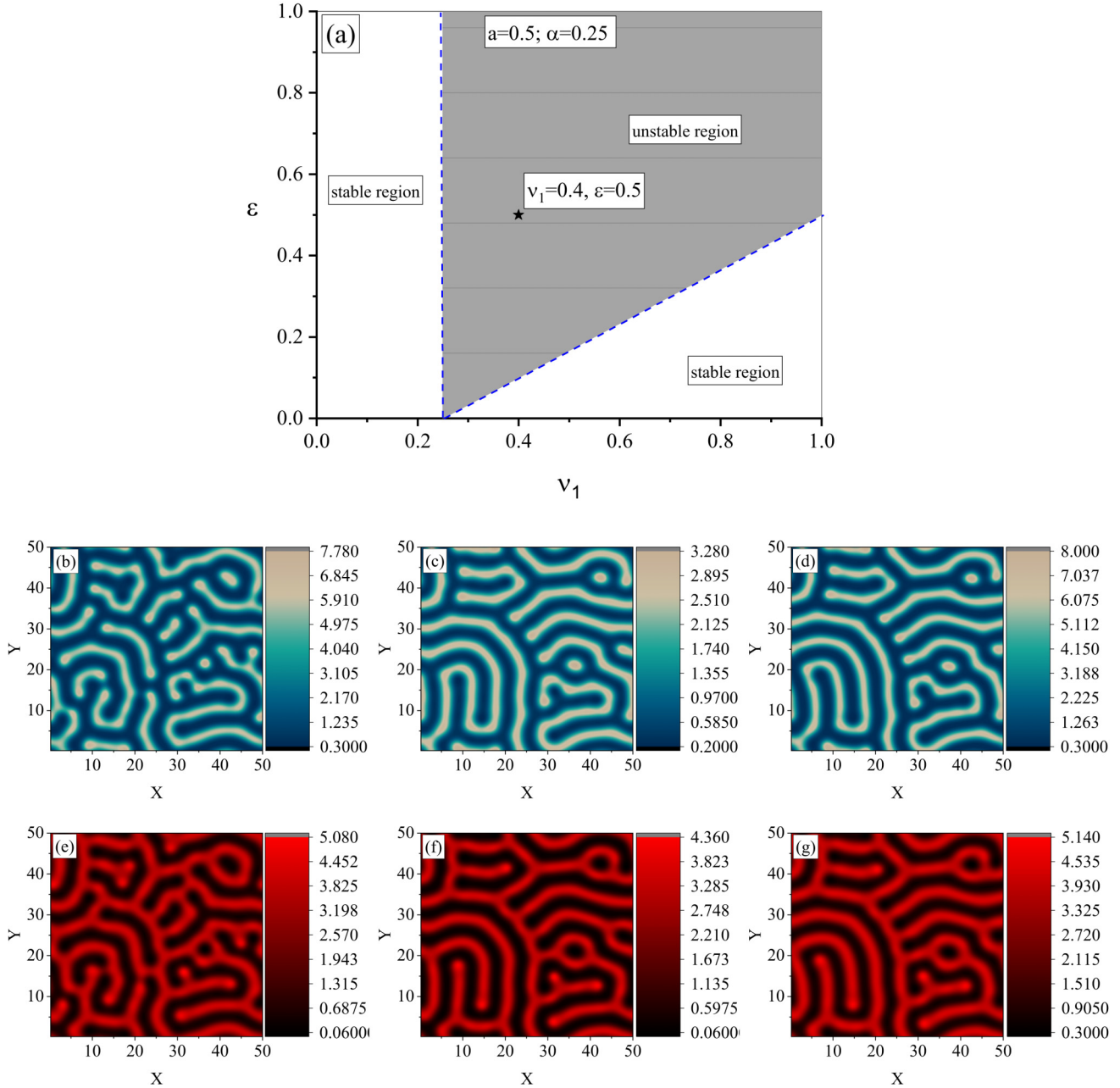


FIG. 8. Same as in Fig. 7 but for $\alpha = 0.25$ (units arbitrary).

First, the case where the inhibitor of the primary layer is subjected to the parametric forcing and the activators of both the layers undergo coupling, i.e.,

$$\text{Primary layer} \begin{cases} \frac{\partial u_1}{\partial t} = \frac{u_1^2}{v_1} - u_1 + \phi_1 + \alpha(u_1 - u_2) + D_1 \nabla^2 u_1 \\ \frac{\partial v_1}{\partial t} = \mu_1 \{u_1^2 - v_1 [1 - a \sin(\omega_p t)]\} + \nabla^2 v_1 \end{cases}, \tag{3.36}$$

$$\text{Secondary layer} \begin{cases} \frac{\partial u_2}{\partial t} = \frac{u_2^2}{v_2} - u_2 + \phi_2 + \alpha(u_2 - u_1) + D_2 \nabla^2 u_2 \\ \frac{\partial v_2}{\partial t} = \mu_2 (u_2^2 - v_2) + \nabla^2 v_2 \end{cases}. \tag{3.37}$$

Full numerical simulation of the Eqs. (3.36) and (3.37) reveals no patterned state, which can be explained as follows: In this situation we have applied the parametric forcing which plays the key role for inducing instability in the inhibitor component of the primary layer. It may be noted that the inhibitor diffuses faster than activator even in absence of forcing. The application of

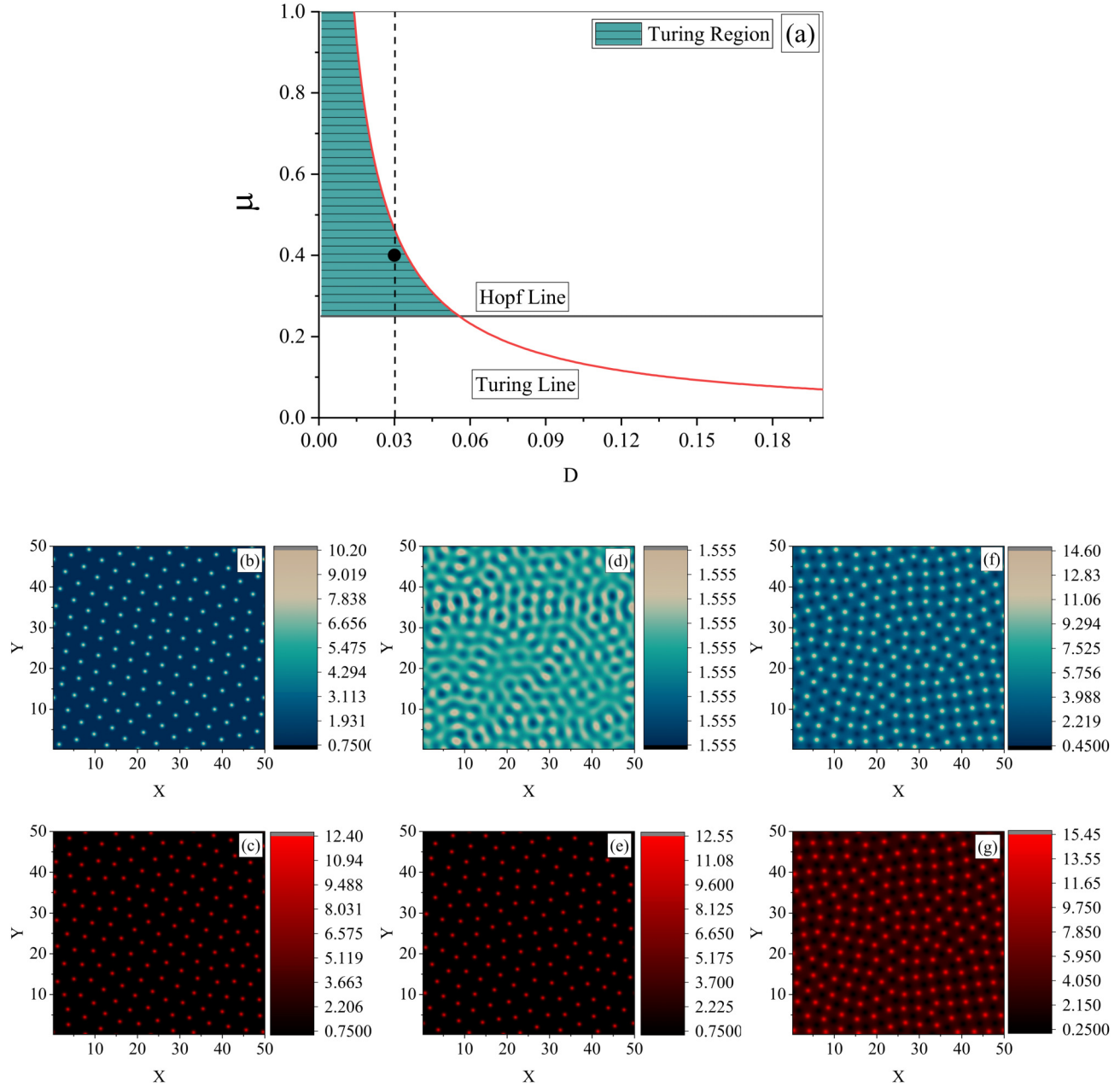


FIG. 9. (a) Bifurcation diagram for the coupled Gierer-Meinhardt model without parametric forcing. The Hopf line (black line) and the Turing line (red line) are shown in the μ - D parameter space for $\phi_1 = \phi_2 = \phi = 0.6$ and $D_1 = D_2 = D$ (units arbitrary). The parameters $\mu_1 = \mu_2 = \mu = 0.6$ and $D_1 = D_2 = D = 0.03$ are chosen in the Turing region for the primary and the secondary layers. [(b) and (c)] Spatiotemporal profiles of (b) u_1 (primary layer) and (c) u_2 (secondary layer) obtained by numerical simulation of parametrically driven Gierer-Meinhardt reaction-diffusion system [Eqs. (3.34) and (3.35)] at $t = 5000$ time units for $\alpha = 0.0$ and $a = 0.12$. [(d) and (e)] Same as in (b) and (c) but for $a = 0.13$. The upper layer tends to loose spatial heterogeneity as compared to the lower layer. [(f) and (g)] Same as in (d) and (e) but for $\alpha = 0.3$. The spatiotemporal patterns reappear in both layers (units arbitrary).

parametric forcing causes a further enhancement of the diffusion so that the parametric instability condition cannot be sustained because of rapid homogenization of the system.

In the second scenario we have applied the coupling to the inhibitor and parametric forcing to the activator.

$$\text{Primary layer} \begin{cases} \frac{\partial u_1}{\partial t} = \frac{u_1^2}{v_1} - u_1[1 - a \sin(\omega_p t)] + \phi_1 + D_1 \nabla^2 u_1 \\ \frac{\partial v_1}{\partial t} = \mu_1(u_1^2 - v_1) + \alpha(v_1 - v_2) + \nabla^2 v_1 \end{cases}, \tag{3.38}$$

$$\text{Secondary layer} \begin{cases} \frac{\partial u_2}{\partial t} = \frac{u_2^2}{v_2} - u_2 + \phi_2 + D_2 \nabla^2 u_2 \\ \frac{\partial v_2}{\partial t} = \mu_2(u_2^2 - v_2) + \alpha(v_2 - v_1) + \nabla^2 v_2 \end{cases}. \tag{3.39}$$

The numerical simulation of Eqs. (3.38) and (3.39) again reveals no patterned state. The forcing of activator leads to its enhancement of effective diffusion in the first layer as compared to that of the inhibitor. As the diffusive coupling terms are applied to the inhibitors of the system the disparity of the diffusion in the activator and inhibitor gets reduced which prevents the propagation of the instability and the system remains homogeneous.

Third, we consider a situation when both the forcing and the coupling terms are present in the inhibitor,

$$\text{Primary layer} \quad \begin{cases} \frac{\partial u_1}{\partial t} = \frac{u_1^2}{v_1} - u_1 + \phi_1 + D_1 \nabla^2 u_1 \\ \frac{\partial v_1}{\partial t} = \mu_1 \{u_1^2 - v_1 [1 - a \sin(\omega_p t)]\} + \alpha(v_1 - v_2) + \nabla^2 v_1 \end{cases}, \quad (3.40)$$

$$\text{Secondary layer} \quad \begin{cases} \frac{\partial u_2}{\partial t} = \frac{u_2^2}{v_2} - u_2 + \phi_2 + D_2 \nabla^2 u_2 \\ \frac{\partial v_2}{\partial t} = \mu_2 (u_2^2 - v_2) + \alpha(v_2 - v_1) + \nabla^2 v_2 \end{cases}. \quad (3.41)$$

In this case the instability generated by the parametric forcing dies down readily due to the large effective diffusion coefficient of the inhibitor of the first layer. It is therefore imperative that the system would prefer homogeneity. This has been corroborated by numerical simulation of Eqs. (3.40) and (3.41). We have also numerically simulated Eqs. (3.34) and (3.35) where the parameter set is chosen in such a way that initially both the activator and the inhibitor of the primary layer are in the oscillatory state. In this scenario also, the simulations did not produce any relevant patterned state.

Summarizing all the aforesaid cases, we therefore conclude that a balanced interplay of parametric forcing and coupling which act in opposite directions in the activator dynamics characterized by slow diffusion can give rise to parametric instability and synchrony in the system.

IV. CONCLUSION

In this paper we have demonstrated a type of synchrony in sustained chemical oscillations and in spatiotemporal patterns in the coupled reaction-diffusion systems arising out of parametric instability. The synchronized parametric oscillation due to periodic forcing of a parameter is quite distinct from the usual direct driving of the dynamics that leads to quasiperiodic oscillation of the system since in absence of the driving the system returns to the usual oscillatory state or the Hopf state. In parametric oscillation one observes sustained oscillation without decay at a frequency half the pumping frequency once the strength of periodic forcing is kept above the instability threshold, while below the threshold the system undergoes decay to the homogeneous steady state. We now summarize the main conclusions of this study. First, antiphase synchronization of oscillations or spatiotemporal patterns in the two layers depend on the critical threshold of coupling strength as well as the critical threshold of the strength of forcing under parametric resonance condition. Second, the dispersion relation, i.e., the dependence of the allowed range of wavelength for synchrony in spatiotemporal patterns on excitation frequency, is determined by the critical coupling strength as well as the

amplitude of external forcing. The multiscale perturbation theory clearly reveals the parametric instability regions in V-shaped Arnold tongue in the scaled amplitude-frequency plot. The region of instability gets enlarged with decrease of the strength of coupling. Third, while the linear stability analysis based on perturbation theory reveals the generic features of the conditions for parametric instability-induced synchrony in oscillations or patterns, the details of the nature of patterns depend on the specificity of the model considered and the nonlinearity intrinsic to the model itself. Fourth, our scheme is based on the coupling between two layers. It is possible to include more layers to the primary one to achieve synchrony among them although such a generalization becomes difficult because of increased number of equations to be solved to derive analytically the critical thresholds for forcing strength and strength of coupling between different layers. Fifth, the numerical simulations carried out using the parameters of the system residing in the Turing region of the bifurcation diagram reveals that the parametric forcing strength and the coupling strength act in different directions in the activator dynamics, i.e., while the coupling strength assists the process of pattern formation, the parametric forcing strength plays a destructive role.

In view of the direct bearing of the multilayer tissues and lipid bilayer membranes, the multilayer chemical systems with or without diffusion can prove themselves to be interesting candidates for the study of complex patterns [41] in biological systems. Further investigation in this direction may throw more light on synchronization in biosystems.

ACKNOWLEDGMENTS

Thanks are due to University Grant Commission, Government of India, for a Fellowship (S.P.); to DBT-RA Program in Biotechnology and Life Sciences, Government of India (K.P.); and to Science and Engineering Research Board, the Department of Science and Technology, Government of India, for J. C. Bose National Fellowship under Grant No. SB/S2/JCB-030/2015 for partial financial support.

[1] J. Aguirre, R. L. Viana, and M. A. F. Sanjuán, *Rev. Mod. Phys.* **81**, 333 (2009); J. K. Bhattacharjee, A. K. Mallik, and S. Chakraborty, *Ind. J. Phys.* **81**, 1115 (2007).

[2] S. H. Strogatz, *Non-linear Dynamics and Chaos: With Applications to Physics, Biology, Chemistry, and Engineering* (Perseus Books, Reading, MA, 1994); I. R. Epstein and J. A. Pojman, *An*

- Introduction to Non-linear Chemical Dynamics: Oscillations, Waves, Patterns, and Chaos* (Oxford University Press, Oxford, 1998); J. K. Bhattacharjee, S. Chakraborty, and A. K. Mallik, *Nonlinear Dynamics Primer: with Applications to Magnetohydrodynamics* (Prism Books, Bangalore, 2011).
- [3] D. L. Gonzalez and O. Piro, *Phys. Rev. Lett.* **50**, 870 (1983); T. Nomura and L. Glass, *Phys. Rev. E* **53**, 6353 (1996); L. Glass, Y. Nagai, K. Hall, M. Talajic, and S. Nattel, *ibid.* **65**, 021908 (2002); I. Z. Kiss, Y. Zhai, and J. L. Hudson, *Phys. Rev. Lett.* **94**, 248301 (2005).
- [4] L. Glass and R. Perez, *Phys. Rev. Lett.* **48**, 1772 (1982); N. F. Pedersen and A. Davidson, *Phys. Rev. B* **41**, 178 (1990); V. Eckhouse, M. Fridman, N. Davidson, and A. A. Friesem, *Phys. Rev. Lett.* **100**, 024102 (2008).
- [5] C. A. Czeisler, J. S. Allan, S. H. Strogatz, J. M. Ronda, R. Sanchez, C. D. Rios, W. O. Freitag, G. S. Richardson, and R. E. Kronauer, *Science* **233**, 667 (1986).
- [6] C. Gronfier, K. P. Wright Jr., R. E. Kronauer, and C. A. Czeisler, *Proc. Natl. Acad. Sci. USA* **104**, 9081 (2007).
- [7] L. Glass, *Nature* **410**, 277 (2001); K. P. Wright, A. W. McHill, B. R. Birks, B. R. Griffin, T. Rusterholz, and E. D. Chinoy, *Curr. Bio.* **23**, 1554 (2013).
- [8] A. L. Lin, M. Bertram, K. Martinez, H. L. Swinney, A. Ardelea, and G. F. Carey, *Phys. Rev. Lett.* **84**, 4240 (2000); A. L. Lin, A. Hagberg, E. Meron, and H. L. Swinney, *Phys. Rev. E* **69**, 066217 (2004).
- [9] V. K. Vanag, A. M. Zhabotinsky, and I. R. Epstein, *Phys. Rev. Lett.* **86**, 552 (2001).
- [10] I. Sgura, B. Bozzini, and D. Lacitignola, *AIP Conf. Proc.* **1493**, 896 (2012).
- [11] A. Yochelis, A. Hagberg, E. Meron, A. L. Lin, and H. L. Swinney, *SIAM J. Appl. Dyn. Syst.* **1**, 236 (2012); O. Steinbock, V. Zykov, and S. C. Müller, *Nature* **366**, 322 (1993); R. M. Mantel and D. Barkley, *Phys. Rev. E* **54**, 4791 (1996).
- [12] A. Karma and V. S. Zykov, *Phys. Rev. Lett.* **83**, 2453 (1999); A. L. Lin, A. Hagberg, A. Ardelea, M. Bertram, H. L. Swinney, and E. Meron, *Phys. Rev. E* **62**, 3790 (2000).
- [13] I. Berenstein and Y. D. Decker, *J. Chem. Phys.* **143**, 064105 (2015).
- [14] M. C. Cross and P. C. Hohenberg, *Rev. Mod. Phys.* **65**, 851 (1993); S. S. Riaz and D. S. Ray, *Indian J. Phys.* **81**, 1177 (2007); R. Kapral, and K. Showalter, *Chemical Waves and Patterns* (Kluwer Academic, Alphen aan den Rijn, 1995); M. Cross and H. Greenside, *Pattern Formation and Dynamics in Nonequilibrium Systems* (Cambridge University Press, Cambridge, UK, 2009).
- [15] M. Eiswirth and G. Ertl, *Phys. Rev. Lett.* **60**, 1526 (1988); S. Rüdiger, D. G. Míguez, A. P. Muñozuri, F. Sagués, and J. Casademunt, *ibid.* **90**, 128301 (2003); S. Ghosh and D. S. Ray, *Eur. Phys. J. B* **88**, 180 (2015).
- [16] Q. Gao, J. Li, K. Zhang, and I. R. Epstein, *Chaos* **19**, 033134 (2009); A. O. León, M. G. Clerc, and S. Coulibaly, *Phys. Rev. E* **91**, 050901(R) (2015); J. Porter, I. Tínao, A. Laverón-Simavilla, and J. Rodríguez, *ibid.* **88**, 042913 (2013).
- [17] D. W. Jordan and P. Smith, *Nonlinear Ordinary Differential Equations* (4th ed.) (Oxford University Press, Oxford, 2007).
- [18] M. Faraday, *Philos. Trans. R. Soc. Lond.* **121**, 299 (1831); H. M. Jaeger, S. R. Nagel, and R. P. Behringer, *Rev. Mod. Phys.* **68**, 1259 (1996); A. O. Maksimov and T. G. Leighton, *Proc. R. Soc. Lond. A* **468**, 57 (2012).
- [19] F. Melde, *Ann. Phys.* **185**, 193 (1860); L. Rayleigh, *Philos. Mag.* **15**, 229 (1883); C. S. Liu and V. K. Tripathi, *Phys. Rev. B* **70**, 115414 (2004); A. Ahmad and V. K. Tripathi, *ibid.* **72**, 193409 (2005).
- [20] L. Rayleigh, *Theory of Sound* (2nd ed.) (Dover, New York, 1945).
- [21] T. G. Roer, *Microwave Electronic Devices* (Springer Science, Dordrecht, 1996).
- [22] A. Yariv, *Quantum Electronics* (3rd ed.) (John Wiley & Sons, New York, 1989).
- [23] N. F. Pedersen, M. R. Samuelsen, and K. Saermark, *J. Appl. Phys.* **44**, 5120 (1973).
- [24] S. Ghosh and D. S. Ray, *J. Chem. Phys.* **143**, 124901 (2015).
- [25] G. Bard Ermentrout and J. Rinzel, *J. Math. Bio.* **11**, 269 (1981); S. Ghosh and D. S. Ray, *Phys. Rev. E* **93**, 032209 (2016).
- [26] V. K. Vanag, L. Yang, M. Dolnik, A. M. Zhabotinsky, and I. R. Epstein, *Nature* **406**, 389 (2000).
- [27] S. Nkomo, M. R. Tinsley, and K. Showalter, *Phys. Rev. Lett.* **110**, 244102 (2013).
- [28] J. F. Totz, R. Snari, D. Yengi, M. R. Tinsley, H. Engel, and K. Showalter, *Phys. Rev. E* **92**, 022819 (2015).
- [29] M. Dolnik and I. R. Epstein, *Phys. Rev. E* **54**, 3361 (1996).
- [30] L. Yang and I. R. Epstein, *Phys. Rev. Lett.* **90**, 178303 (2003).
- [31] A. V. Panfilov, R. H. Keldermann, and M. P. Nash, *Phys. Rev. Lett.* **95**, 258104 (2005).
- [32] D. Dab, J. P. Boon, and Y. X. Li, *Phys. Rev. Lett.* **66**, 2535 (1991).
- [33] K. Ohno, T. Ogawa, and N. J. Suematsu, *Phys. Rev. E* **99**, 012208 (2019).
- [34] A. J. Catllá, A. McNamara, and C. M. Topaz, *Phys. Rev. E* **85**, 026215 (2012).
- [35] L. Zhang, S. Zhang, H. Tong, D. Lei, and B. Hu, *Phys. Rev. E* **79**, 056213 (2009).
- [36] H. Yang and J. Yang, *Phys. Rev. E* **76**, 016206 (2007).
- [37] L. Ji and Q. S. Li, *J. Chem. Phys.* **123**, 094509 (2005).
- [38] I. I. Blekhman, *Synchronization in Science and Technology* (ASME Press, New York, 1988).
- [39] A. Gierer and H. Meinhardt, *Kybernetik* **12**, 30 (1972); H. Meinhardt and A. Gierer, *J. Cell Sci.* **15**, 321 (1974).
- [40] A. Bhattacharyay and J. K. Bhattacharjee, *Phys. Lett. A* **358**, 121 (2006); S. Ghosh, S. Paul, and D. S. Ray, *Phys. Rev. E* **94**, 042223 (2016); S. Paul, S. Ghosh, and D. S. Ray, *ibid.* **94**, 062217 (2016).
- [41] R. A. Barrio, C. Varea, J. L. Aragón, and P. K. Maini, *Bull. Math. Biol.* **61**, 483 (1999).